

SENSOR FUSION FOR DISTRIBUTED INERTIAL MEASUREMENT UNITS

Su Yeon Choi^{ID*}, Holly Dinkel^{ID*,†}, David Hanley^{ID‡}, and Timothy Bretl^{ID*},

This work demonstrates the reduction of Angle Random Walk (ARW), Velocity Random Walk (VRW), and Rate Random Walk (RRW) through sensor fusion of complementary distributed Inertial Measurement Units (IMUs) for robot and satellite navigation. High-fidelity IMUs may violate the tight cost, mass, power, and volume constraints typical of small robot and satellite platforms. Low-cost Micro-Electromechanical System (MEMS) IMUs may have performance characteristics unsuitable for attitude estimation when used alone in a system. In this work, the measurements of multiple MEMS IMUs are fused into a virtual IMU. The fusion algorithm takes time-synchronized measurements from an arbitrary number of sensors and produce one virtual measurement estimate. Allan variance is used to evaluate ARW, VRW, and RRW noise performance for the estimated angular velocity and linear acceleration measurements. The noise performance of the virtual sensor measurement estimates and of the single-sensor measurements is compared. Sensor fusion is demonstrated with the simulated data of up to 18 MEMS IMUs and for real data collected by 5 MEMS IMUs. A tradeoff between number of sensors and noise reduction performance is presented to aid the design of future scalable, distributed inertial measurement systems.

INTRODUCTION

The performance of MEMS gyroscopes degrades over time due to high noise and stochastic drift. This work reduces noise and bias for a scalable system of distributed gyroscopes. By scalable, we mean that a user can choose to include an arbitrary number of inertial sensors beyond the minimal number of sensors required for inertial navigation (3 gyroscopes and 3 accelerometers). To provide users with additional design capabilities, this system is also distributed, which means that sensors can be placed arbitrarily by the user as needed in their design and as constrained by observability and noise requirements.

Such a scalable and distributed system offers several advantages over existing IMU designs. First, this technology gives space-constrained systems the advantage of redundancy for fault detection, isolation, and recovery (FDIR). An IMU that can survive, detect, and isolate faults is particularly useful in a space environment where MEMS technology is particularly prone to failure.¹ Previous work looked at optimal IMU sensor placement for FDIR in theory² and for larger non-distributed units.³ A scalable and distributed solution introduces a need to build on existing fault detection and isolation algorithms for this type of sensor; it also requires that optimal sensor configurations be revisited in the context of additional placement constraints that a designer may have. As an example of the kind of value this technology provides, consider the geostationary SWIMSat mission, which

^{*}University of Illinois Urbana-Champaign, Urbana, IL, USA.

[†]NASA Ames Research Center, Moffett Field, CA, USA.

[‡]University of Edinburgh, Edinburgh, United Kingdom

is intended to monitor coronal mass ejections and meteor impacts from a 6U CubeSat. This satellite is more susceptible than CubeSats in lower orbits to failure caused by radiation.⁴ Different MEMS IMU components respond differently to radiation depending on factors such as actuation type and sensor geometry.^{1,5} A distributed and scalable IMU can reduce environmental risks to spacecraft operations and mitigate other in-use failures such as electrostatic discharge.

A second benefit of the proposed system is that it can allow for the direct measurement of angular acceleration. It has been shown that the use of many accelerometers to directly measure angular acceleration without the differentiation of gyroscope measurements can be beneficial to state estimation because noise amplification caused by differentiation can be avoided.⁶ Concepts like the NASA commercial in-space robotic assembly and services (CIRAS) mission involve the construction of truss structures in orbit. Prior research acknowledges errors in truss construction propagate with the length of the truss.⁷ Improved measurement of the angular acceleration of the spacecraft can result in better system identification (particularly of the resulting moment of inertia) of the resulting constructed structure. This improved system identification can result in better attitude control of the constructed component as well as better attitude control of the spacecraft during the construction process.

A final advantage of this IMU system is it can provide additional design flexibility. For example, volume is a significant concern in the design of space robotic systems. Collocated IMUs consume a fixed volume that may be hard to integrate—in effect, adding design constraints. Because a distributed IMU can be split into multiple pieces, its volume may be easier to integrate. CubeSats are systems for which this sort of flexibility in layout could be important. The distributed architecture admits changing mission profiles and adds redundancy to the navigation system.

An example of the kind of mission that this navigation system can help enable is the European Space Agency’s SILEX mission, which was the first mission demonstrate the possibility of transferring significant amounts of data from LEO to GEO via inter-satellite links.⁸ Rather than store information onboard until the next opportunity for ground-station downlink, satellites enabled by optical communication can transmit data immediately to other satellites which can forward it to ground users. Satellite mega-constellations, including SpaceX’s Starlink and Amazon’s Kuiper constellations, can only achieve agile data transmission through inter-satellite links which minimize communication latency. Optical communication has strict acquisition, tracking, and pointing requirements which necessitate very accurate state estimation.⁹ Future missions using optical communications could benefit from a scalable and distributed IMU technology to improve attitude determination and control.

In this work, the measurements of the distributed IMU system are fused as a virtual IMU.^{10,11} Fusion takes time-synchronized angular velocity and linear acceleration measurements from an arbitrary number of IMUs and outputs one angular velocity and specific force. Allan variance is used to estimate noise parameters for the fused estimates which are compared to the single-sensor noise. Sensor fusion is demonstrated with the simulated data of up to 18 IMUs and for real data collected by 5 MEMS IMUs. A tradeoff between number of sensors and noise reduction performance is presented to aid the design of future scalable, distributed inertial measurement systems. Data and source code are publicly released at github.com/schoi355/multi_imu_fusion.

Table 1: Estimated ARW, VRW, and RRW parameters for noise compared to quoted values

Parameter	Tactical-Grade IMU ¹⁸	MEMS IMU ^{19,20}	Virtual IMU
$\sigma_{g,ARW}$ ($^{\circ}/\sqrt{s}$)	1.50×10^{-3}	3.33×10^{-3}	1.27×10^{-3}
$\sigma_{a,VRW}$ ($m/s/\sqrt{s}$)	1.30×10^{-3}	$*4.70 \times 10^{-3}$	2.73×10^{-3}
$\sigma_{g,RRW}$ ($^{\circ}/s/\sqrt{Hz}$)	2.0×10^{-3}	1.80×10^{-2}	6.24×10^{-3}
$\sigma_{a,RRW}$ ($m/s^2/\sqrt{Hz}$)	1.57×10^{-4}	7.36×10^{-4}	3.70×10^{-4}

* The datasheet does not provide the $\sigma_{a,VRW}$ parameter. The parameter was obtained from a static test by collecting measurements from this sensor while it laid stationary on a table.

RELATED WORK

Previous research suggests sensor fusion could reduce the total noise of output measurements for a scalable system of IMUs. In one study with a cluster of 32 gyros and 16 accelerometers, root mean square noise was reduced by a factor of three through simply averaging angular rate and specific force measurements across the group as compared to single sensors.¹² In an experiment with a redundant IMU (12 accelerometers and 12 gyroscopes), a Generalized Autoregressive Conditional Heteroskedasticity (GARCH) model combining measurements was able to reduce the output gyroscope sensor noise by 56.2% compared to a single individual IMU.¹³ In a separate study, measurements from an array of six gyroscopes were combined with a Kalman filter. The Allan variance of the measurements was computed and a first order Markov process model resulted in a noise density reduction of 72.7%, angle random walk reduction of 70.3%, rate random walk reduction of 59.0%, and bias instability reduction of 69.8% in a static test.¹⁴ In work studying accelerometer-only IMUs, accelerometers in certain configurations are used to measure angular velocity as well as specific force.¹⁵ Given the freedom to arrange gyroscopes and accelerometers in such a coupled manner, this work builds on both areas of previous work to improve IMU performance. This substantial improvement in IMU performance is known to translate into improved state estimation performance of integrated systems as well as improved performance of the inertial navigation system alone. In fact, recent work in the area of monocular visual-inertial navigation derived a direct relationship between the bias instability in an IMU and the potential state estimation accuracy of such a system.¹⁶ In a recent report to the CubeSat developers conference, IMU bias instability could justify investing in tactical-grade IMUs ($\sim \$5,000$) for CubeSats instead of far cheaper MEMS IMUs ($\sim \$50$) more commonly used on robotic platforms.¹⁷

METHODOLOGY

This section describes the method of sensor fusion with multiple distributed IMUs. Sensor fusion solves for $\hat{\omega}_{i,m}$ and $\hat{\mathbf{a}}_{i,m}$ using stochastic optimization with the least-squares estimator, where $\hat{\omega}_{i,m}$ and $\hat{\mathbf{a}}_{i,m}$ are the measurement estimates of angular rate and specific force for the system at time t . The measurements of the i^{th} gyroscope and the accelerometer are denoted as $\omega_{i,m}$ and $\mathbf{s}_{i,m}$, respectively. The i^{th} accelerometer and gyroscope are assumed to be co-located and are assumed to be distributed throughout a rigid body which cannot bend or warp. The inertial reference frame of the i^{th} IMU, $\{I_i\}$, moves with respect to a global reference frame, $\{G\}$. The gyroscope and accelerometer measurements, $\omega_{i,m}, \mathbf{a}_{i,m} \in \mathbb{R}^3$, are a function of their true angular velocity and

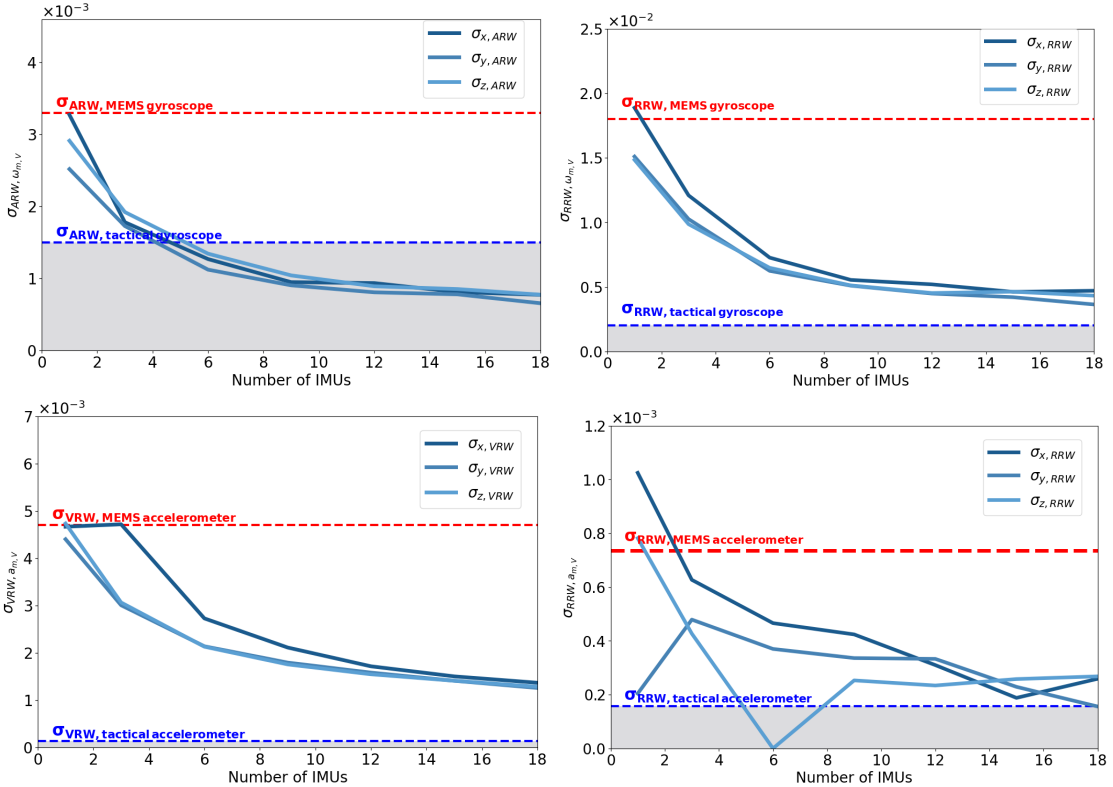


Figure 1: The parameters for ARW ($\sigma_{g,ARW}$), VRW ($\sigma_{a,VRW}$), and RRW ($\sigma_{g,RRW}$, $\sigma_{a,RRW}$) of the virtual IMU are analyzed based on the number of IMUs used for the fusion of the angular velocity and linear acceleration measurements. The $\sigma_{g,ARW}$ outperforms the performance of a tactical-grade gyroscope when more than four IMUs are fused. $\sigma_{g,RRW}$, $\sigma_{a,VRW}$, and $\sigma_{a,RRW}$ improves as the number of IMUs increases, though their performance remains below that of tactical-grade IMU.

linear acceleration, ${}^{I_i}\boldsymbol{\omega}_i$ and ${}^G\mathbf{a}_i$, as

$$\boldsymbol{\omega}_{i,m} = {}^{I_i}\boldsymbol{\omega}_i + \mathbf{b}_{i,g} + \mathbf{n}_{i,g}, \quad \mathbf{n}_{i,g} \sim \mathcal{N}(0, \sigma_{i,g}^2 \mathbf{I}_3) \quad (1)$$

$$\mathbf{a}_{i,m} = {}^{I_i}\mathbf{R}_G({}^G\mathbf{a}_i - {}^G\mathbf{g}) + \mathbf{b}_{i,a} + \mathbf{n}_{i,a}, \quad \mathbf{n}_{i,a} \sim \mathcal{N}(0, \sigma_{i,a}^2 \mathbf{I}_3) \quad (2)$$

where ${}^{I_i}\mathbf{R}_G$ is the rotation from $\{G\}$ to $\{I_i\}$, \mathbf{n}_g and \mathbf{n}_a are white Gaussian noises corrupting the gyroscope and accelerometer measurements, \mathbf{b}_g and \mathbf{b}_a are the gyroscope and accelerometer measurement biases modeled as random walk processes, and ${}^G\mathbf{g}$ is the gravity vector in the global frame.^{10,11}

$$\mathbf{b}_{i,g,t} = \mathbf{b}_{i,g,t-1} + \mathbf{n}_{i,\omega g}, \quad \mathbf{n}_{i,\omega g} \sim \mathcal{N}(0, \sigma_{i,\omega g}^2 \mathbf{I}_3) \quad (3)$$

$$\mathbf{b}_{i,a,t} = \mathbf{b}_{i,a,t-1} + \mathbf{n}_{i,\omega a}, \quad \mathbf{n}_{i,\omega a} \sim \mathcal{N}(0, \sigma_{i,\omega a}^2 \mathbf{I}_3) \quad (4)$$

$$(5)$$

Given synchronized measurements for rigidly connected IMUs $i = 1, \dots, N$, one of the IMUs can be used to establish a virtual IMU reference frame, $\{I_v\}$, and extrinsic calibration returns the transformation between the i^{th} IMU and the virtual IMU v , $({}^{I_i}\mathbf{R}_{I_v}, {}^{I_v}\mathbf{p}_{I_i})$. The virtual IMU

measurements are generated as¹¹

$${}^{I_v}\boldsymbol{\omega}_{v,m} = \mathbf{N}^+ \boldsymbol{\omega}_m \quad (6)$$

$${}^{I_v}\mathbf{a}_{v,m} = \mathbf{T}(\mathbf{a}_m - \mathbf{S}(\boldsymbol{\omega}_{v,m})) \quad (7)$$

where

$$\mathbf{N} = \begin{bmatrix} {}^{I_1}\mathbf{R}_{I_v} \\ {}^{I_2}\mathbf{R}_{I_v} \\ \vdots \\ {}^{I_N}\mathbf{R}_{I_v} \end{bmatrix}, \quad \mathbf{Y} = \begin{bmatrix} {}^{I_1}\mathbf{R}_{I_v} \lfloor {}^{I_v}\mathbf{p}_{I_1} \rfloor_{\times} \\ {}^{I_2}\mathbf{R}_{I_v} \lfloor {}^{I_v}\mathbf{p}_{I_2} \rfloor_{\times} \\ \vdots \\ {}^{I_N}\mathbf{R}_{I_v} \lfloor {}^{I_v}\mathbf{p}_{I_N} \rfloor_{\times} \end{bmatrix}, \quad \mathbf{T} = (\mathbf{Z}^T \mathbf{N})^+ \mathbf{Z}^T, \quad (8)$$

$$\boldsymbol{\omega}_m = \begin{bmatrix} \boldsymbol{\omega}_{1,m} \\ \boldsymbol{\omega}_{2,m} \\ \vdots \\ \boldsymbol{\omega}_{N,m} \end{bmatrix}, \quad \mathbf{a}_m = \begin{bmatrix} \mathbf{a}_{1,m} \\ \mathbf{a}_{2,m} \\ \vdots \\ \mathbf{a}_{N,m} \end{bmatrix}, \quad \mathbf{S}(\cdot) = \begin{bmatrix} {}^{I_1}\mathbf{R}_{I_v} \lfloor \cdot \rfloor_{\times}^2 {}^{I_v}\mathbf{p}_{I_1} \\ {}^{I_2}\mathbf{R}_{I_v} \lfloor \cdot \rfloor_{\times}^2 {}^{I_v}\mathbf{p}_{I_2} \\ \vdots \\ {}^{I_N}\mathbf{R}_{I_v} \lfloor \cdot \rfloor_{\times}^2 {}^{I_v}\mathbf{p}_{I_N} \end{bmatrix}, \quad (9)$$

\mathbf{Z}^T is left nullspace projection of \mathbf{Y} , $\lfloor \cdot \rfloor_{\times}$ is the skew-symmetric matrix, and \mathbf{A}^+ is the Moore-Penrose inverse of \mathbf{A} , defined as

$$\mathbf{A}^+ = (\mathbf{A}^T \mathbf{A})^{-1} \mathbf{A}^T. \quad (10)$$

For $\mathbf{x}_v = [{}^G\bar{\mathbf{q}}_v^T, \mathbf{b}_{v,g}^T, {}^G\mathbf{v}_v^T, \mathbf{b}_{v,a}^T, {}^G\mathbf{p}_v^T]^T \in \mathbb{R}^{16 \times 1}$, the IMU state can be propagated to predict a state estimate, $\hat{\mathbf{x}}_v$, as²¹

$$\hat{\mathbf{x}}_v = f(\hat{\mathbf{x}}, \boldsymbol{\omega}_{v,m}, \mathbf{a}_{v,m}). \quad (11)$$

EXPERIMENTS

This section describes the experiments and results obtained from sensor fusion. First, simulated IMU measurements are used to generate a virtual IMU and a scalability study is performed using these synthetic data to compare noise performance between a single tactical-grade IMU, a single MEMS IMU, and the virtual IMU. Next, real measurements from a system of multiple MEMS IMUs are fused and used for IMU state propagation to demonstrate its application to state estimation.

Simulated Measurements

The first goal of this work is to determine whether a virtual IMU fusing measurements of multiple MEMS IMUs can achieve noise levels comparable to a single tactical-grade IMU. In experiments with simulated data, Angle Random Walk (ARW), Velocity Random Walk (VRW), and Rate Random Walk (RRW) are introduced into simulated measurements collected by $N = 6$ IMUs stationary on a table with a constant angular velocity of $[0, 0, 0]^\circ/\text{s}$ and a constant acceleration of $[0, 0, 9.81] \text{ m/s}^2$. The standard deviations for noise components for the MEMS IMUs and tactical-grade IMU are based on the specifications from datasheets.^{18–20} Because the ARW parameter for the MEMS gyroscope is not specified in the datasheet, measurements from a static test of a real sensor were collected and the ARW parameter was obtained from the Allan variance curve. Computing the Allan variance for the measurements synthesized for the Virtual IMU returns the parameters for ARW, $\sigma_{g,ARW}$, VRW, $\sigma_{a,VRW}$, and RRW, $\sigma_{g,RRW}$ and $\sigma_{a,RRW}$.²² As shown in Table 1, the noise level of the virtual gyroscope outperforms a tactical-grade gyroscope for ARW. For VRW, the virtual accelerometer outperforms the MEMS accelerometer but falls short of the tactical-grade accelerometer. The noise level of the Virtual IMU also outperforms the MEMS IMU but not the

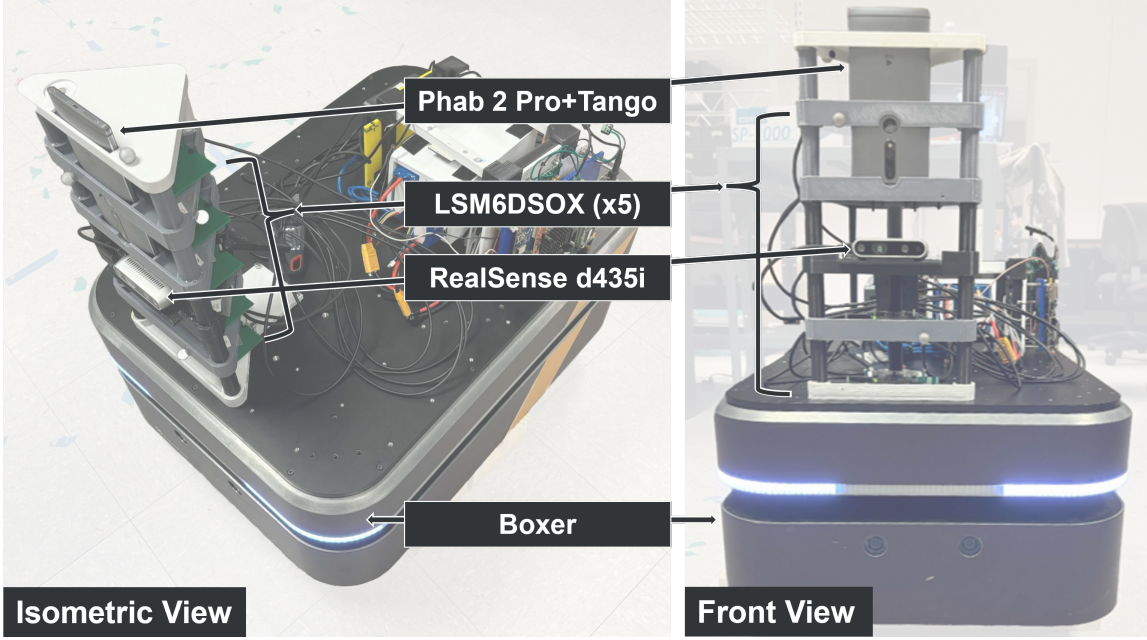


Figure 2: Five IMUs, one RGBD camera, and a device running Google Tango are mounted on a mobile robot to collect data for sensor fusion and navigation algorithm testing.

tactical-grade IMU for RRW. Although the virtual IMU fusing multiple MEMS IMU measurements underperforms the tactical-grade IMU, it achieves noise parameters at the same order of magnitude as the tactical-grade IMU, something which a single MEMS IMU cannot achieve, at a fraction of the sensor cost.

In a second scalability study, measurements of up to $N = \{1, \dots, 18\}$ IMUs are synthesized as a virtual IMU. In these experiments, all of these IMUs have the same orientation and are spaced evenly, 0.1m apart, along the x , y , and z axes to form a cube. Computing the Allan variance for the virtual IMU returns its noise parameters. Figure 1 presents the noise parameters for the virtual gyroscope and accelerometer as the number of IMUs used for sensor fusion increases. The virtual gyroscope outperforms the tactical-grade gyroscope in terms of angle random walk when $N \geq 4$. For velocity random walk and rate random walk, the virtual IMU did not achieve tactical-grade performance, but significantly reduced noise levels as compared to a single MEMS IMU. This indicates fusing multiple IMUs can serve as a practical alternative to using a tactical-grade IMU.

Real Measurements

The second goal of this work is to determine whether a virtual IMU fusing measurements from multiple MEMS IMUs can improve state estimation over a single MEMS sensor. The multiple MEMS IMU data are collected using the Clearpath Boxer ground wheeled robot. A testing platform with $N = 5$ layered STMicroelectronics LSM6DSOX IMUs with 7.62cm spacing is used for data collection.²³ Both intrinsic and extrinsic calibrations are performed using the Kalibr toolbox.²⁴ The IMUs at each level collected measurements at approximately 100Hz. Data from the IMUs are first transmitted to a microcontroller and then to a single board computer mounted on the robot. The onboard computer is accessed remotely during data collection using a remote desktop application.

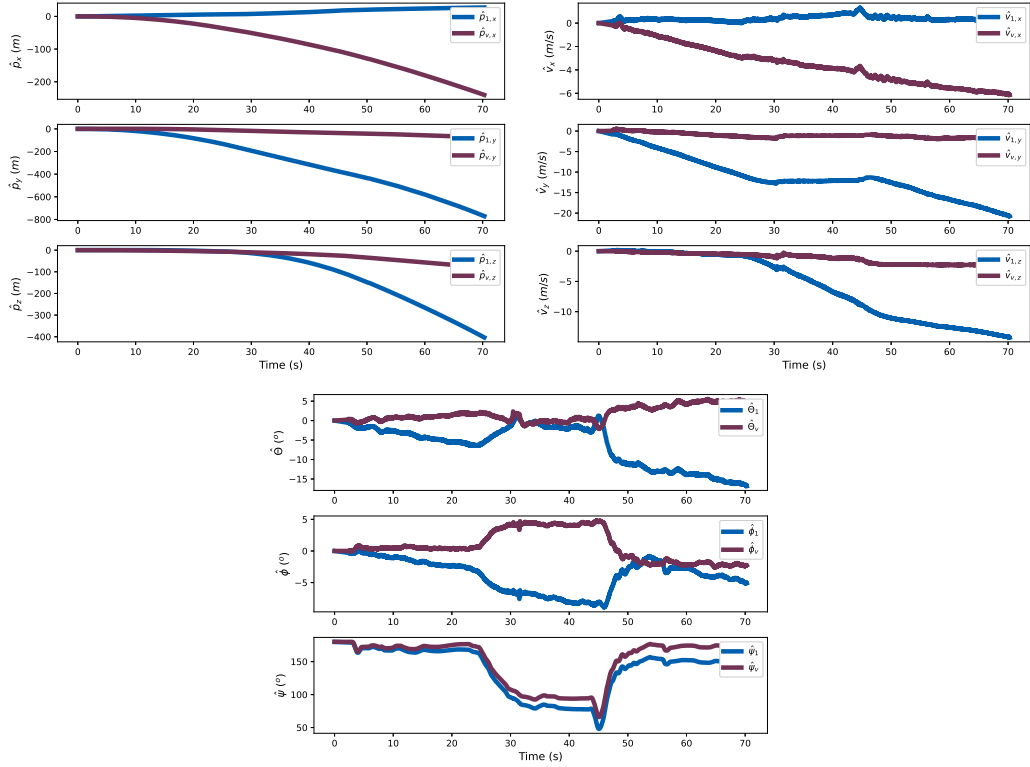


Figure 3: Comparing state estimation of a single MEMS IMU to the virtual IMU fusing measurements from five real sensors on data collected with the ground robot in a hallway demonstrates the significant deviation and error accumulation IMU-only state estimation introduces.

A Lenovo Phab 2 Pro running Google Tango is used as a reference visual inertial navigation system for ground truth trajectory information for future integration of the virtual IMU into Visual-Inertial Odometry (VIO). Time-stamped images from an Intel Realsense D435i camera are also collected for use in VIO. This testing platform is shown in 2.

The measurements of the MEMS IMUs on this testing platform are collected as the ground robot testing platform is driven through the hallway of a building. These measurements are fused into a measurement for the virtual IMU. The measurements for the virtual IMU and for a single MEMS IMU on the test platform are each used to estimate the state of the ground robot. The state estimates for the single IMU and virtual IMU are compared in Figure 3.

CONCLUSION

This work presented a method of fusing multiple IMU measurements as a virtual IMU to provide an estimated measurement for the entire system. This method of fusing measurements reduces measurement noise at the system level through scaling the number of IMUs. Noise levels of the virtual IMU outperformed noise levels of a single MEMS IMU, and demonstrated comparable performance to the tactical-grade IMU. Future work will incorporate visual information from the RealSense camera into state estimation using visual-inertial odometry²⁵ and compare the impact of sensor fusion on localization performance for the VIO system. This kind of system could be useful for future small satellites or robots to reduce navigation system costs without sacrificing attitude estimation

accuracy.

ACKNOWLEDGMENTS

The authors thank Jongwon Lee, Parth Shrotri, Shivani Atre, Achintya Gahalaut, Chen Li, Ali Albazroun, Jiho Sim, Chris Schreiber, Geonwoo Kim, and Katherine Ruiz for assistance with data collection from the testing platform of MEMS IMUs used in experiments. The authors thank Mayank Mittal for assisting with improving the figures presented in this manuscript. The authors also thank the developers of the open-source software used in this work.^{22,26–30} NASA contract 80NSSC18P2132 and 80NSSC20C0020 funded this work. Holly Dinkel was supported by NASA Space Technology Graduate Research Opportunity award 80NSSC21K1292, a P.E.O. Scholar Award, and the Zonta International Amelia Earhart Fellowship.

AUTHORS



Su-Yeon Choi is pursuing a Ph.D. in Aerospace Engineering at the University of Illinois Urbana-Champaign. She received the M.S. in Aerospace Engineering at the Georgia Institute of Technology and the B.S. in Mathematics at the Korea Military Academy. She has been serving in the Republic of Korea Army since 2010.



Holly Dinkel is pursuing a Ph.D. in Aerospace Engineering at the University of Illinois Urbana-Champaign as a NASA Space Technology Graduate Research Fellow with the NASA Ames Research Center Intelligent Robotics Group. She received the M.S. in Aeronautics and Astronautics from Stanford University and the B.S. in Chemical Engineering and B.A. in Music from the University of Missouri.



David Hanley is a Postdoctoral Research Associate with the School of Informatics Centre for Inflammation Research at the University of Edinburgh. He received the Ph.D. in Electrical and Computer Engineering, the M.S. in Aerospace Engineering, and the B.S. in Aerospace Engineering at the University of Illinois Urbana-Champaign.



Timothy Bretl is a Professor of Aerospace Engineering and a Research Professor with the Coordinated Science Laboratory at the University of Illinois Urbana-Champaign. He was previously a Postdoctoral Fellow with the Department of Computer Science at Stanford University and also completed the Ph.D. and M.S. in Aeronautics and Astronautics at Stanford University. He received the B.S. in Engineering and the B.A. in Mathematics from Swarthmore College.

REFERENCES

- [1] H. R. Shea, “Effects of Radiation on MEMS,” *Reliability, Packaging, Testing, and Characterization of MEMS/MOEMS and Nanodevices X*, Vol. 7928, SPIE, 2011, pp. 96–108.
- [2] M. Jafari, “Optimal Redundant Sensor Configuration for Accuracy Increasing in Space Inertial Navigation System,” *Aerospace Sci. Technol.*, Vol. 47, 2015, pp. 467–472.
- [3] S. Sukkarieh, P. Gibbens, B. Grocholsky, K. Willis, and H. Durrant-Whyte, “A Low-Cost Redundant Inertial Measurement Unit for Unmanned Air Vehicles,” *Int. J. Robot. Res.*, Vol. 19, 01 2000, pp. 1089–1103.

- [4] V. Hernandez, P. Gankidi, A. Chandra, A. Miller, P. Scowen, H. Barnaby, E. Adamson, E. Asphaug, and J. Thangavelautham, “SWIMSSat: Space Weather and Meteor Impact Monitoring using a Low-Cost 6U CubeSat,” 2016.
- [5] A. L. Hartzell, M. G. Da Silva, and H. R. Shea, *MEMS Reliability*. Springer Science & Business Media, 2010.
- [6] P. Schopp, H. Graf, W. Burgard, and Y. Manoli, “Self-Calibration of Accelerometer Arrays,” *IEEE Trans. Instrum. Meas.*, Vol. 65, No. 8, 2016, pp. 1913–1925.
- [7] E. Komendera and N. Correll, “Precise Assembly of 3D Truss Structures Using MLE-Based Error Prediction and Correction,” *Int. J. Robot. Res.*, Vol. 34, No. 13, 2015, pp. 1622–1644.
- [8] E. Perez, M. Bailly, and J. Pairo, “Pointing Acquisition And Tracking System For Silex Inter Satellite Optical Link,” *Proceedings of SPIE, Acquisition, Tracking, and Pointing III*, Vol. 1111, 09 1989.
- [9] H. Hemmati, *Deep Space Optical Communications*. John Wiley & Sons, 2006.
- [10] K. Eckenhoff, P. Geneva, and G. Huang, “Sensor-Failure-Resilient Multi-IMU Visual-Inertial Navigation,” *IEEE Int. Conf. Robot. Autom. (ICRA)*, 2019, pp. 3542–3548.
- [11] M. Zhang, X. Xu, Y. Chen, and M. Li, “A Lightweight and Accurate Localization Algorithm Using Multiple Inertial Measurement Units,” *IEEE Robot. Autom. Lett.*, Vol. 5, No. 2, 2020, pp. 1508–1515.
- [12] D. Greenheck, R. Bishop, E. Jonardi, and J. Christian, “Design and Testing of a Low-Cost MEMS IMU Cluster for Smallsat Applications,” *AIAA/USU Conference on Small Satellites*, 2014, pp. 1–10.
- [13] A. Waegli, J. Skaloud, S. Guerrier, M. E. Parés, and I. Colomina, “Noise Reduction and Estimation in Multiple Micro-Electro-Mechanical Inertial Systems,” *Meas. Sci. Technol.*, Vol. 21, No. 6, 2010, p. 065201.
- [14] C. Jiang, L. Xue, H. Chang, G. Yuan, and W. Yuan, “Signal Processing of MEMS Gyroscope Arrays to Improve Accuracy Using a 1st Order Markov for Rate Signal Modeling,” *Sensors*, Vol. 12, No. 2, 2012, pp. 1720–1737.
- [15] S. Park and S. K. Hong, “Angular Rate Estimation Using a Distributed Set of Accelerometers,” *Sensors*, Vol. 11, No. 11, 2011, pp. 10444–10457.
- [16] J. Hernandez, K. Tsotsos, and S. Soatto, “Observability, Identifiability and Sensitivity of Vision-Aided Inertial Navigation,” *IEEE Int. Conf. Robot. Autom. (ICRA)*, 2015, pp. 2319–2325.
- [17] F. Azure, R. Hevner, and W. Holemans, “Lessons Learned Measuring 3U and 6U Payload Rotation and Velocity when Dispensed in Reduced Gravity Environment,” *12th Annual CubeSat Workshop*, 2015.
- [18] Analog Devices, “Tactical Grade Inertial Measurement Unit (IMU) with Industry’s Lowest SWaP+C,” 2024. Datasheet.
- [19] STMicroelectronics, “Ultrawide Bandwidth, Low-Noise, 3-Axis Digital Vibration Sensor,” 2023. Datasheet DS12569 Rev 7.
- [20] Silicon Sensing, “Pinpoint Precision Navigation and Pointing Gyroscope CRM100 Technical Datasheet,” 2023. Datasheet CRM100-00-0100-132 Rev 10.
- [21] J. Hol, *Sensor Fusion and Calibration of Inertial Sensors, Vision, Ultra-Wideband and GPS*. Linkopings Universitet (Sweden), 2011.
- [22] N. Mayorov and D. Sidorov, “Allan Variance,” GitHub, 2024.
- [23] D. Hanley, A. S. D. d. Oliveira, X. Zhang, D. H. Kim, Y. Wei, and T. Bretl, “The Impact of Height on Indoor Positioning With Magnetic Fields,” *IEEE Trans. Instrum. Meas.*, Vol. 70, 2021, pp. 1–19.
- [24] P. Furgale, J. Rehder, and R. Siegwart, “Unified Temporal and Spatial Calibration for Multi-Sensor Systems,” *IEEE/RSJ Int. Conf. Intell. Robot. Sys. (IROS)*, IEEE, 2013, pp. 1280–1286.
- [25] C. Campos, R. Elvira, J. J. G. Rodríguez, J. M. Montiel, and J. D. Tardós, “ORB-SLAM3: An Accurate Open-Source Library for Visual, Visual–Inertial, and Multimap SLAM,” *IEEE Trans. Robot.*, Vol. 37, No. 6, 2021, pp. 1874–1890.
- [26] C. R. Harris, J. Millman, S. v. d. Walt, R. Gommers, P. Virtanen, D. Cournapeau, E. Wieser, J. Taylor, S. Berg, N. J. Smith, R. Kern, M. Picus, S. Hoyer, M. H. v. Kerkwijk, M. Brett, A. Haldane, J. F. d. Río, M. Wiebe, P. Peterson, P. Gérard-Marchant, K. Sheppard, T. Reddy, W. Weckesser, H. Abbasi, C. Gohlke, and T. E. Oliphant, “Array Programming with NumPy,” *Nature*, Vol. 585, 2020, pp. 357–362.
- [27] P. Virtan, R. Gommers, T. E. Oliphant, M. Haberland, T. Reddy, D. Cournapeau, E. Burovski, P. Peterson, W. Weckesser, J. Bright, *et al.*, “Scipy 1.0: Fundamental Algorithms for Scientific Computing in Python,” *Nat. Methods*, Vol. 17, 2020, pp. 261—272.
- [28] J. D. Hunter, “Matplotlib: A 2D Graphics Environment,” *Comput. Sci. Eng.*, Vol. 9, No. 3, 2007, pp. 90–95.

- [29] T. Kluyver, B. Ragan-Kelley, F. Pérez, B. Granger, M. Bussonnier, J. Frederic, K. Kelley, J. Hamrick, J. Grout, S. Corlay, P. Ivanov, D. Avila, S. Abdalla, and C. Willing, “Jupyter Notebooks – A Publishing Format for Reproducible Computational Workflows,” *Positioning and Power in Academic Publishing: Players, Agents and Agendas* (F. Loizides and B. Schmidt, eds.), IOS Press, 2016, pp. 87 – 90.
- [30] W. McKinney, “Data Structures for Statistical Computing in Python,” *Proceedings of the 9th Python in Science Conference*, 2010, pp. 56–61.